

Article

Direct Conversion of Ethanol to Propylene over Zn-Modified HBeta Zeolite: Influence of Zinc Precursors

Ting Bai ¹, Xiaohui Li ¹ , Liang Ding ¹ , Jin Wang ¹, Yong-Shan Xiao ^{2,*} and Bin Cao ^{1,*}

¹ College of Chemistry and Chemical Engineering, Xi'an Shiyou University, No. 18, East Dianzier Road, Xi'an 710065, China

² School of Chemistry & Chemical Engineering, Shaanxi Normal University, No. 620, West Chang'an Avenue, Xi'an 710119, China

* Correspondence: xiaoy@snnu.edu.cn (Y.-S.X.); caobinxys@126.com (B.C.)

Abstract: A series of Zn-modified HBeta (Zn/HBeta) catalysts were prepared via the wetness impregnation method with different zinc precursors such as ZnSO₄·7H₂O, ZnCl₂, C₄H₆O₄Zn·2H₂O and Zn(NO₃)₂·6H₂O, and their catalytic performance in the conversion of ethanol to propylene reaction was evaluated. Results indicate that the amount and strength distribution of the acid sites of the Zn/HBeta catalysts were easily tuned by employing different types of zinc precursors. More importantly, when the zinc species were introduced to the HBeta, the propylene yield was significantly enhanced, whereas the yields of ethylene and C₂–C₄ alkanes were remarkably suppressed. For the catalyst prepared by using the ZnCl₂ precursor, a higher propylene yield of up to 43.4% for Zn/HBeta-C was achieved as a result of the moderate amount and strength distribution of acid sites. The average coking rate of the used Zn/HBeta catalysts strongly depended on the amount of total acid sites, especially the strong acid sites, i.e., the higher the amount of total acid sites of the catalyst, the greater the average coking rate. For the catalyst prepared by using the ZnSO₄·7H₂O precursor, Zn/HBeta-S exhibited a better stability even after depositing more coke, which was due to the higher amount of strong acid sites.

Keywords: ethanol; propylene; HBeta zeolite; zinc precursors; acidity; coke deposition



Citation: Bai, T.; Li, X.; Ding, L.; Wang, J.; Xiao, Y.-S.; Cao, B. Direct Conversion of Ethanol to Propylene over Zn-Modified HBeta Zeolite: Influence of Zinc Precursors. *Catalysts* **2024**, *14*, 276. <https://doi.org/10.3390/catal14040276>

Academic Editors: Roberto Fiorenza and Antonio Eduardo Palomares

Received: 14 March 2024

Revised: 15 April 2024

Accepted: 17 April 2024

Published: 19 April 2024



Copyright: © 2024 by the authors. Licensee MDPI, Basel, Switzerland. This article is an open access article distributed under the terms and conditions of the Creative Commons Attribution (CC BY) license (<https://creativecommons.org/licenses/by/4.0/>).

1. Introduction

Propylene is widely used in the production of highly valuable chemicals such as polypropylene, acrylonitrile, propylene oxide, acetone and so on [1–3]. Propylene is mainly produced as co-product from naphtha steam cracking and catalytic cracking, which are strongly dependent on fossil fuels [4]. In addition, methanol-to-propylene (MTP) and propane dehydrogenation (PDH) processes have been developed using nonpetroleum resources [5,6]. Nevertheless, the production of propylene is still in short supply owing to the increasing demand for its derivatives. With the shortage of fossil fuels and environmental protection, the conversion of bio-ethanol to propylene has attracted much attention in recent years, since bio-ethanol production technology has been rapidly developed. The ethanol-to-propylene reaction (ETP) is considered to be a carbon-neutral process, which can reduce the damage to the environment and relieve the pressure of oil shortages [7–9].

To date, catalysts for the ETP reaction are mainly concentrated on zeolites and transition metal oxides. For the acidic zeolites such as HZSM-5, ethanol is first dehydrated to produce ethylene on acid sites, followed by oligomerization–cracking reactions to form propylene as a result of shape selectivity [10–14]. However, the randomness of the ethylene oligomerization reaction results in a propylene yield of around 20–30%. Meanwhile, side reactions such as aromatization, cyclization and hydrogen transfer easily occur on the strong acid sites, giving rise to extensive coke deposition and fast deactivation of the catalyst [9,15]. Alternatively, transition metal oxides also have gained substantial attention for the ETP reaction [16–18]. Iwamoto et al. [19,20] found that a propylene yield of 30% was achieved

over Y/CeO₂ in the presence of water, and a similar propylene yield of 34% was observed on Sc/In₂O₃ [21]. Xia et al. [18] reported that a propylene yield of 44% was achieved over Y/ZrO₂. The stability of metal oxides in the ETP reaction is significantly improved because of the lower coke deposition than with zeolites. However, a large amount of ethylene, of 20–32%, was also produced as a result of the weak acid sites and the absence of shape selectivity of the zeolite [20,21]. Thus, it is still a great challenge to develop a catalyst with a higher propylene yield and better stability.

Recently, metal oxide–zeolite composites for the ETP reaction have been proposed for combining the merits of zeolite and metal oxide [22–25], which has been demonstrated to be an effective strategy for improving the propylene yield and stability of the catalyst. Typically, a relatively high propylene yield over the In₂O₃-beta composite can be kept stable at about 50% for 46 h under a reaction temperature of 460 °C and a weight hourly space velocity (WHSV) of 0.2 h^{−1} [22]. Unfortunately, the expensive In₂O₃ precursor may limit its large-scale preparation for industrial application. In this regard, after optimizing the ratios of Si/Al and ZnCeO_x to HBeta zeolite, the composite of ZnCeO_x and HBeta zeolite exhibits a higher propylene yield of more than 55% and an ethylene yield of 3% under the optimal reaction conditions, and the propylene yield remains stable at around 50% after three generation cycles [23]. These significant results can lay a solid foundation for the rational and controllable design of metal oxide–zeolite composites with higher propylene yield and better stability. As is well known, metal precursors play a crucial role in the preparation of metal oxide catalysts [26,27]. However, to the best of our knowledge, the effect of metal precursors on hybrid catalysts in the ETP reaction has not been systematically investigated. There is still a lack of a clear and good understanding of the effect of the metal precursors. To this end, it is necessary to investigate the influence of metal precursors on metal oxide–zeolite composites in the ETP reaction.

In this work, a series of Zn/HBeta catalysts were prepared using different zinc precursors such as ZnSO₄·7H₂O, ZnCl₂, C₄H₆O₄Zn·2H₂O and Zn(NO₃)₂·6H₂O. The physico-chemical properties of the fresh and used catalysts were characterized by X-ray diffraction (XRD), temperature programmed desorption of ammonia (NH₃-TPD), N₂ adsorption-desorption, Fourier-transform infrared spectroscopy (FTIR) and temperature programmed oxidation (TPO). The catalytic performance of the Zn/HBeta catalysts in the ETP reaction was investigated. Based on the obtained results, the influence of zinc precursors on the acidic properties, catalytic performance and coke deposition of Zn/HBeta catalysts were rigorously elucidated.

2. Results

2.1. Structural and Textural Properties

The XRD patterns of the HBeta and Zn/HBeta catalysts are shown in Figure 1. A series of prominent diffraction peaks at 2θ of 7.8, 12.0, 13.6, 21.0, 22.4, 29.4 and 41.0° were observed for the HBeta and Zn/HBeta catalysts, which are typical characteristics of the BEA structure of zeolite [24]. Compared with HBeta, the peaks of the BEA structure of Zn/HBeta were lower to different degrees, suggesting the crystallinity of the Zn/HBeta catalysts is lower than HBeta. This is attributed to the coverage of zinc species on HBeta [22]. Moreover, a series of diffraction peaks at 18.5, 26.2, 26.9, 29.2, 34.9, 35.6, 38.5 and 41.0° assigned to the ZnSO₄ (JCPDS 33-1476) were observed for Zn/HBeta-S, indicating the presence of a significant quantity of ZnSO₄ on the surface of Zn/HBeta-S [28]. Since the initial decomposition temperature of ZnSO₄ to ZnO·ZnSO₄ was around 700 °C, most of the ZnSO₄ compound on Zn/HBeta-S was well retained after calcination at 450 °C for 4 h [29]. In contrast, strong diffraction peaks at 31.7, 34.4, 36.2 and 47.5° corresponding to the (100), (002), (101) and (102) lattice planes of ZnO (JCPDS 36-1451) were obviously detected on both Zn/HBeta-Ac and Zn/HBeta-N, suggesting the presence of large-sized and well-crystallized ZnO [30]. Moreover, the diffraction peaks of ZnO of Zn/HBeta-N was stronger than that of Zn/HBeta-Ac, indicating that the crystallite size of ZnO was larger.

There were no diffraction peaks of the detectable zinc species for Zn/HBeta-C, indicating the existence of highly dispersed ZnO.

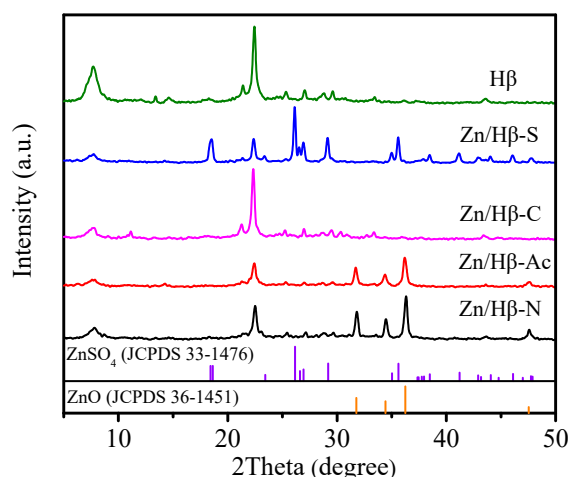


Figure 1. XRD patterns of HBeta and Zn/HBeta catalysts.

Table 1 shows the textural properties of the HBeta and Zn/HBeta catalysts. The BET specific surface area (S_{BET}) and total pore volume (V_{total}) of HBeta were $560.6 \text{ m}^2/\text{g}$ and $0.36 \text{ cm}^3/\text{g}$, respectively. In contrast, the Zn/HBeta catalysts showed much lower S_{BET} and V_{total} , i.e., $162.0\text{--}277.2 \text{ m}^2/\text{g}$ for S_{BET} and $0.13\text{--}0.27 \text{ cm}^3/\text{g}$ for V_{total} . More importantly, a significant decline in the micropore volume (V_{micro}) was observed for all of the Zn/HBeta catalysts in comparison with HBeta, while a very similar mesopore volume (V_{meso}) was obtained, except for Zn/HBeta-S and Zn/HBeta-Ac. The V_{meso} of $0.17 \text{ cm}^3/\text{g}$ for Zn/HBeta-Ac was higher than that of HBeta ($0.13 \text{ cm}^3/\text{g}$) as a result of the structure defects and/or the appearance of intercrystalline pores, whereas the V_{meso} of Zn/HBeta-S was almost half that of HBeta. Considering the microporous structure of HBeta, it is well accepted that the high S_{BET} of HBeta is mainly contributed by the micropores [31]. For this reason, the remarkable decrease in both the V_{total} and S_{BET} of the Zn/HBeta catalysts was rigorously attributed to the decrease in the V_{micro} as a result of the partial pore blockage by the zinc species.

Table 1. The textural properties of HBeta and Zn/HBeta catalysts.

Catalysts	S_{BET} (m^2/g)	V_{micro} (cm^3/g)	V_{meso} (cm^3/g)	V_{total} (cm^3/g)
HBeta	560.6	0.23	0.13	0.36
Zn/HBeta-S	162.0	0.06	0.07	0.13
Zn/HBeta-C	216.7	0.09	0.11	0.20
Zn/HBeta-Ac	248.3	0.10	0.17	0.27
Zn/HBeta-N	277.2	0.12	0.12	0.24

2.2. Acidic Properties

To reveal the acidic properties of the HBeta and Zn/HBeta catalysts, the NH_3 -TPD experiments were conducted, and the results are shown in Figure 2. There are two distinct NH_3 desorption peaks for all of the catalysts. The peaks centered at around $140\text{--}260 \text{ }^\circ\text{C}$ and at about $390\text{--}450 \text{ }^\circ\text{C}$ are assigned to the weak and strong acid sites, respectively. To semi-quantify the varied strengths of the acid sites, the total weak and strong acid sites were determined by integrating the NH_3 desorption peaks, and the corresponding peak areas of the NH_3 desorption is summarized in Table 2. Apparently, irrespective of the total and strong acid sites, the amount of acid sites was decreased in the order Zn/HBeta-S > Zn/HBeta-C > HBeta > Zn/HBeta-Ac > Zn/HBeta-N. Moreover, the amount of strong acid sites of Zn/HBeta-S was four times that of HBeta, which can be reasonably attributed to

the super acidic characteristic of residual ZnSO_4 . For Zn/HBeta-C, the amount of strong acid sites was higher than that of HBeta as a result of the highly dispersed zinc species. For Zn/HBeta-Ac and Zn/HBeta-N, the amount of acid sites is much lower than that of HBeta, regardless of the total weak and strong acid sites, which can be associated with the large-sized ZnO. In contrast, a comparable amount of weak acid sites was observed in the case of Zn/HBeta-S, Zn/HBeta-C and HBeta. Thus, the amount and strength distribution of acid sites on the Zn/HBeta catalysts were simply regulated by introducing different types of zinc precursors.

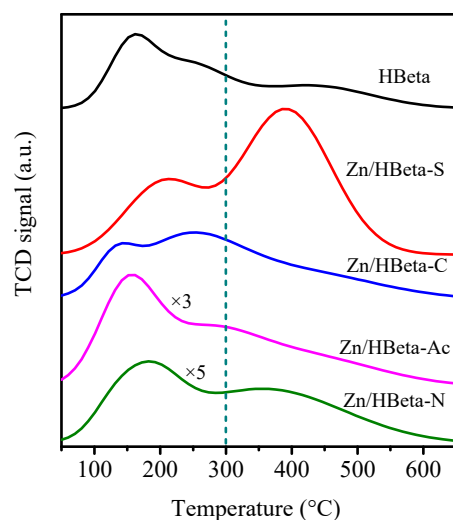


Figure 2. NH_3 -TPD profiles of HBeta and Zn/HBeta catalysts.

Table 2. The acidic properties of HBeta and Zn/HBeta catalysts.

Catalysts	Acidity Distribution (a.u./g)		
	Weak (50–300 °C)	Strong (>300 °C)	Total
HBeta	170.9	91.1	262.0
Zn/HBeta-S	195.6	379.8	575.4
Zn/HBeta-C	187.0	130.8	317.8
Zn/HBeta-Ac	89.4	47.5	136.9
Zn/HBeta-N	41.5	33.9	75.4

2.3. Catalytic Performance

All of the catalysts gave almost 100% ethanol conversion under the reaction conditions of $T = 500\text{ °C}$, $P = 0.1\text{ MPa}$, $P_{\text{C}_2\text{H}_5\text{OH}} = 0.02\text{ MPa}$, $WHSV = 2.8\text{ h}^{-1}$ and $TOS = 1\text{ h}$. However, the product distribution is significantly dependent on the composition of the catalyst. Figure 3 shows the product distribution of the HBeta and Zn/HBeta catalysts in the ETP reaction. Besides the target product of propylene, the hydrocarbons of CH_4 , C_2H_4 , C_4H_8 , $\text{C}_2\text{–C}_4$ alkanes and C_{5+} (liquid phase products, aliphatic and aromatics) were also detected. Interestingly, HBeta gave a yield of ethylene up to 62.4%. It is generally accepted that ethylene is produced by direct dehydration of ethanol. However, the yield of propylene was as low as 7.8%, which is expected to be produced via trimerization of ethylene followed by β -scission. In addition, the HBeta zeolite gave a C_4H_8 yield of 2.8%. There was a 21.1% yield of $\text{C}_2\text{–C}_4$ alkanes, which was produced by olefin hydrogenation and/or hydrogen transfer reactions. To be specific, the yields of C_2H_6 , C_3H_8 and C_4H_{10} were 4.2%, 8.5% and 8.4%, respectively. A small amount of C_{5+} byproducts (5.6%) was produced via sequential steps through ethylene oligomerization, cracking and/or cyclization and hydrogen transfer reactions on the acid sites of the HBeta zeolite. The byproduct of methane could be negligible (less than 0.5%). When the Zn species were introduced into the HBeta zeolite

through impregnation, the yield of propylene was significantly enhanced and followed the order Zn/HBeta-C (43.4%) > Zn/HBeta-N (37.4%) > Zn/HBeta-Ac (29.2%) > Zn/HBeta-S (16.0%). However, the yield of ethylene was lessened and followed the order Zn/HBeta-S (45.9%) > Zn/HBeta-N (34.1%) \approx Zn/HBeta-Ac (33.6%) > Zn/HBeta-C (30.8%). It is quite probable that the trimerization of ethylene followed by β -scission was significantly enhanced on the Zn species, leading to a higher yield of propylene and a lower yield of ethylene. Moreover, the yield of C₂–C₄ alkanes (1.5~4.3%) was also significantly reduced, which is attributed to the fact that the olefin hydrogenation and/or hydrogen transfer reactions were suppressed by the Zn species of the Zn/HBeta catalysts. There was a clear increase in the yield of C₅₊ byproducts, which was from 10.1% for Zn/HBeta-N to 28.8% for Zn/HBeta-S. Based on the above results, the type of zinc precursors has a significant effect on the catalytic reactivity of Zn/HBeta.

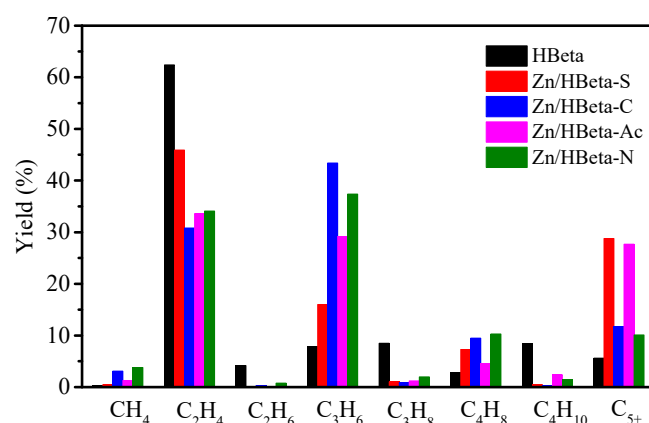


Figure 3. Catalytic performance of HBeta and Zn/HBeta catalysts for the conversion of ethanol to propylene under the conditions of 500 °C, 0.1 MPa, $P_{C_2H_5OH} = 0.02$ MPa, $WHSV = 2.8$ h⁻¹ and TOS = 1 h.

Figure 4 shows the evolution of propylene yield with a TOS of 7 h over the HBeta and Zn/HBeta catalysts in the ETP reaction. The ethanol conversion always remained 100% for all of the catalysts for a TOS of 7 h. The propylene yield of HBeta at TOS = 0.68 h was only 9.3% and gradually declined to 2.0% after a TOS of 7 h. In contrast, Zn/HBeta gave a higher propylene yield than HBeta at the same TOS. The propylene yield at TOS = 0.68 h followed the sequence Zn/HBeta-C (44.9%) > Zn/HBeta-S (38.9%) \approx Zn/HBeta-Ac (38.7%) > Zn/HBeta-N (28.2%). With prolonged TOS, the propylene yield over Zn/HBeta-S, Zn/HBeta-C and Zn/HBeta-Ac gradually declined, while the propylene yield of Zn/HBeta-N was first increased to 35.4% at TOS = 1 h and then decreased to 13.5% at the end of the reaction. Considering the lowest amount of total acid sites of Zn/HBeta-N, the strength distribution of the acid sites might be easily tuned by the deposited coke. The initial small amount of coke deposited on the strong acid sites may lead to the moderate strength distribution of acid sites, giving rise to a maximum yield of propylene. Among these Zn/HBeta catalysts, the lowest decline of the propylene yield was observed for Zn/HBeta-S, and the relatively high propylene yield of 19.0% was still achieved after a TOS of 7 h. It could be concluded that Zn/HBeta-S exhibited a better stability than the other catalysts.

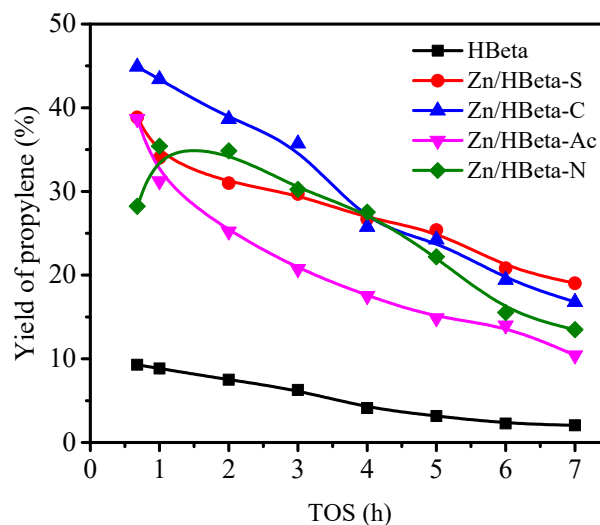


Figure 4. Evolution of propylene yield with TOS over HBeta and Zn/HBeta catalysts in the conversion of ethanol to propylene under the conditions of $T = 500\text{ }^{\circ}\text{C}$, $P = 0.1\text{ MPa}$, $P_{\text{C}_2\text{H}_5\text{OH}} = 0.02\text{ MPa}$ and $WHSV = 2.8\text{ h}^{-1}$.

2.4. Deactivation of the Catalysts

It is widely accepted that coke deposition is the main reason for the deactivation of the zeolite-based catalyst in the ethanol conversion. In this respect, TPO experiments were first conducted to determine the coke species on the used catalysts after a TOS of 7 h. The resultant TPO profiles of the used HBeta and Zn/HBeta catalysts are shown in Figure 5. Clearly, a broad oxygen consumption peak in the temperature region of 350 to 750 $^{\circ}\text{C}$ was observed for all of the catalysts, indicating the presence of the varied types of coke species. Generally, the peak temperature of oxygen consumption is used as a common indicator for identifying the type of coke species, which the peak temperature of the heavier coke species is higher. Meanwhile, to semi-quantitatively determine the amount of coke species, the TPO profiles were deconvoluted into two peaks based on the peak temperature of oxygen consumption. The first peak (Peak I) at around 510–550 $^{\circ}\text{C}$ was attributed to the light coke corresponding to hydrogenated species, while the second peak at around 580–640 $^{\circ}\text{C}$ was assigned to the heavy coke corresponding to carbonaceous species [32]. Thus, the peak temperature (T_{max}) and the corresponding peak area of oxygen consumption are summarized in Table 3.

Table 3. TPO results of used HBeta and Zn/HBeta catalysts.

Used Catalysts	$T_{\text{max}}\text{ (}^{\circ}\text{C)}$		The Consumption of Oxygen (a.u./g)		
	Peak I	Peak II	Peak I	Peak II	Total
HBeta	545	611	25.8	47.5	73.3
Zn/HBeta-S	533	634	64.2	39.7	103.9
Zn/HBeta-C	551	602	54.1	15.4	69.5
Zn/HBeta-Ac	546	603	39.6	19.8	59.4
Zn/HBeta-N	518	580	9.9	33.1	43.0

As shown in Figure 5 and Table 3, it is found that the total oxygen consumption of the used catalysts followed the order Zn/HBeta-S > HBeta > Zn/HBeta-C > Zn/HBeta-Ac > Zn/HBeta-N, indicating the same order of the total coke amount. Specifically, the area of Peak I followed the order Zn/HBeta-S > Zn/HBeta-C > Zn/HBeta-Ac > HBeta > Zn/HBeta-N, while the area of Peak II presented the order HBeta > Zn/HBeta-S > Zn/HBeta-N > Zn/HBeta-Ac > Zn/HBeta-C. Moreover, in the case of Zn/HBeta-C, Zn/HBeta-Ac and HBeta, a similar peak temperature of Peak I at around 550 $^{\circ}\text{C}$ was achieved, which was higher than those of Zn/HBeta-S and Zn/HBeta-N. This indicated the presence of the

heavier coke species. However, a different order occurred at the peak temperature of Peak II. For HBeta, Zn/HBeta-C and Zn/HBeta-Ac, a similar peak temperature of Peak II at around 600–610 °C was observed, which was lower than that of Zn/HBeta-S (633 °C) but higher than that of Zn/HBeta-N (580 °C).

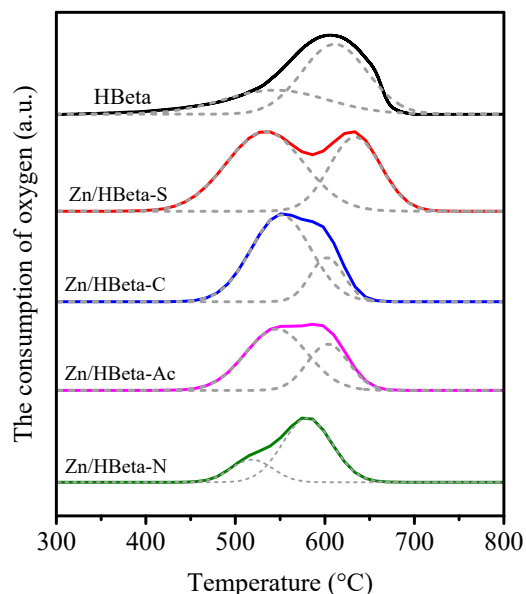


Figure 5. TPO profiles of used HBeta and Zn/HBeta catalysts.

To further study the composition of the deposited coke, FTIR spectra of both fresh and used catalysts were recorded in the regions of 1300–1800 and 2800–3000 cm^{-1} , respectively, and the results are presented in Figure 6. The adsorbed water observed at the band of 1637 cm^{-1} appeared for all of the catalysts [33]. Compared with the fresh catalysts, many new bands were observed for the used catalysts. The assignment of the new bands was as follows: 1355 and 1456 cm^{-1} , corresponding to the CH_3 bending vibrations of aliphatics; 1590 cm^{-1} , corresponding to polyaromatic hydrocarbons and condensed coke; 1618 cm^{-1} , corresponding to dienes and $\text{C}=\text{C}$ double bonds in carbon chains; 2852 and 2870 cm^{-1} , respectively, corresponding to the symmetric vibrations of CH_2 and CH_3 groups; and 2925 and 2958 cm^{-1} , corresponding to the asymmetric vibrations of the same groups [33–35].

The used HBeta zeolite showed a higher intensity of the band at 1590 cm^{-1} , indicating the presence of a higher proportion of aromatic coke. It could be because the large pore size of HBeta was beneficial for oligomerization, cyclization, aromatization, etc., and resulted in the generation of macromolecular compounds such as polyaromatics. L. Pinard et al. [34] identified the coke species of HBeta in the ethanol conversion as alkylbenzenes, mainly hexamethylbenzenes and alkyl-pyrenes, which were found to be the main compounds in the pores. Compared with HBeta, the Zn/HBeta catalysts exhibited higher intensity of the bands at 1618 cm^{-1} , indicating a higher proportion of olefinic coke. This could be because the channels of HBeta tended to be narrow after impregnation, giving rise to the inhibition of polyaromatics formation during the reaction. Furthermore, both 1590 and 1618 cm^{-1} bands were higher for the used Zn/HBeta-S than the other used catalysts, indicating the presence of more olefinic and aromatic coke. This might be mainly attributed to the highest amount of strong acid sites on Zn/HBeta-S. It can be reasonably explained that the ethene oligomerization, cyclization, aromatization, condensation and hydrogen transfer reactions would occur preferentially on strong acid sites.

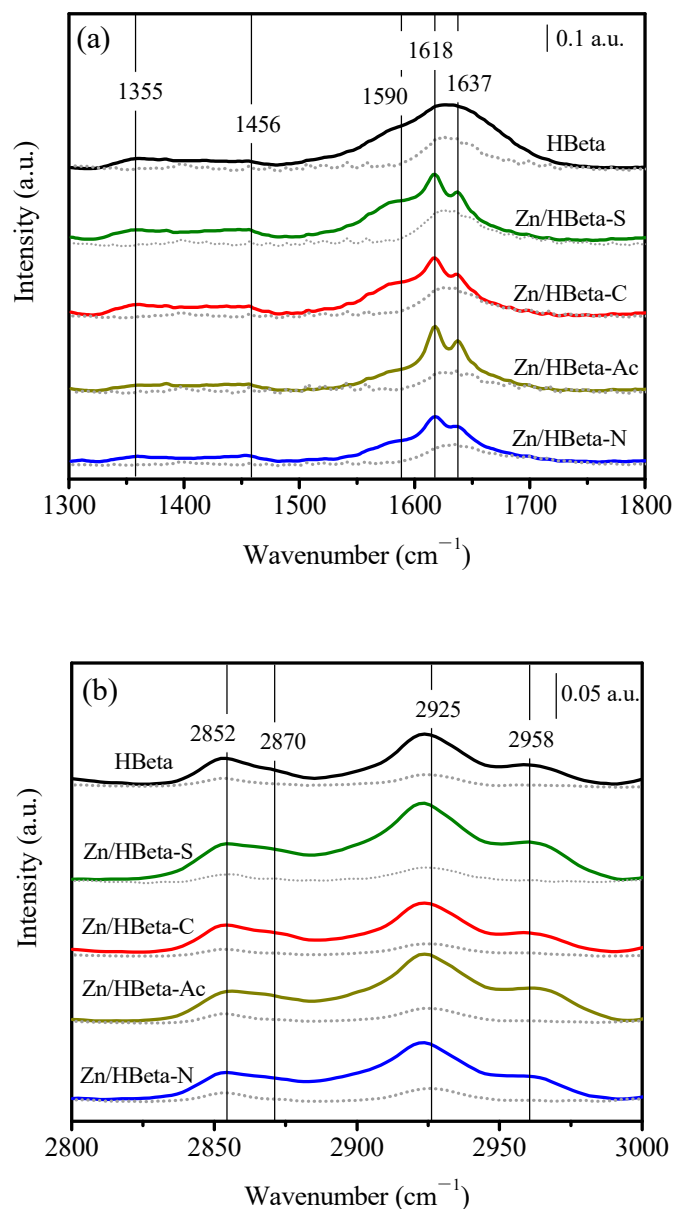


Figure 6. FTIR spectra of both fresh (short dot line) and used (solid line) HBeta and Zn/HBeta catalysts in the regions of 1300–1800 (a) and 2800–3000 cm^{-1} (b).

3. Discussion

3.1. Key Factors Effecting the Catalytic Activity

As is well known, the catalytic performance of the zeolite in the ETP reaction is closely related to the amount and strength distribution of acid sites [13,22]. The reaction pathway is generally accepted to be that ethanol is first dehydrated to produce ethylene, followed by oligomerization–cracking to produce propylene [10–12]. Taking the randomness of the oligomerization into account, the propylene yield is below 20–30%, and the main byproducts are ethylene, butenes, C_2 – C_4 alkanes and C_{5+} hydrocarbons. Expectedly, HBeta gave an ethylene yield up to 62.4% and a propylene yield of 7.8% in this work. Simultaneously, a total amount of C_2 – C_4 alkanes of up to 21.1% was yielded by olefin hydrogenation and/or hydrogen transfer reactions (Figure 3). These results are very consistent with the catalytic activity of HBeta zeolite reported in the literature [22].

Based on the above NH_3 -TPD results, the acidity of Zn/HBeta catalysts could be easily tuned by employing different types of zinc precursors (Figure 2 and Table 2). As a result, the catalytic performance was significantly affected in the ETP reaction. To reveal the effect

of acidity on the catalytic performance of Zn/HBeta, correlation analyses were carried out between both the amount of acid sites and the S/W ratio and the propylene yield, and the results are shown in Figure 7. The S/W ratio represents the ratio of strong acid sites to weak acid sites. However, after careful comparative analysis, there was no direct regular variation pattern between the acidity and the propylene yield. However, based on the fact that Zn/HBeta-C exhibited the highest propylene yield of 43.4% at TOS = 1.0 h, it could be inferred that the moderate amount of acid sites and S/W ratio on Zn/HBeta were more beneficial to the formation of propylene. However, it is difficult to explain why the propylene yield is quite high in the case of the catalysts with a very small amount of acid, e.g., Zn/HBeta-Ac and Zn/HBeta-N. On the other hand, the reaction pathway for Zn/HBeta catalysts might be different from HBeta, according to the previous works. Miao et al. [22] reported that a high yield of propylene up to 50% was achieved for In₂O₃-beta composites by promoting the intermediate of acetone to propylene instead of the byproduct butylene, when the proposed reaction pathway could be ethanol → acetaldehyde → acetone → isopropanol → propylene. Similarly, Zhang et al. [23] proposed the reaction pathway over the composites of ZnCeO_x and HBeta could be ethanol → acetaldehyde → ethyl acetate → acetone → isopropanol → propylene. Moreover, it is found that the basicity of ZnCeO_x plays a vital role for the ethanol dehydrogenation to acetaldehyde, but the acidity of catalysts is more important for the propylene selectivity. Hence, these proposed reaction pathways over the composites of metal oxides and HBeta zeolite are completely different from the HBeta. It was found that large-sized ZnO was clearly observed for Zn/HBeta-Ac and Zn/HBeta-N, and highly dispersed ZnO was presented for Zn/HBeta-C (Figure 1). Since the composition of the above Zn/HBeta catalysts is very similar to the composites of ZnCeO_x and HBeta, as well as the In₂O₃-beta composites, it can be reasonably inferred that a very similar reaction pathway from ethanol to propylene could be proposed for the Zn/HBeta catalysts. However, an exception may occur in the case of Zn/HBeta-S with a great amount of ZnSO₄.

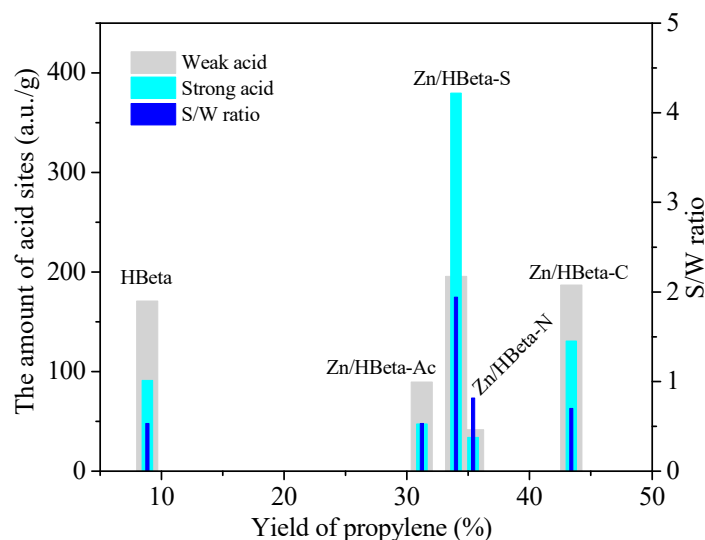


Figure 7. Correlations between acidic properties and propylene yield (TOS = 1 h) of Zn/HBeta catalysts.

Based on the above analysis, it could be concluded that the moderate amount of acid sites and S/W ratio on Zn/HBeta were more beneficial for the formation of propylene in the ETP reaction. The Zn/HBeta catalysts can not only promote the propylene yield from an additional reaction pathway of ethanol → acetaldehyde → acetone → isopropanol → propylene but also suppress the secondary reactions of propylene and the side reactions of key intermediates. Thus, Zn/HBeta exhibited much higher propylene yield compared with HBeta.

3.2. Deactivation Mechanism

The ETP reaction is usually accompanied by a number of side reactions that result in the formation of coke deposition. It is well known that the coke originates from the condensation of intermediates that are also activated by acid sites. To further understand the effect of acidity on the coking behaviors of the used Zn/HBeta catalysts, the amounts of different acid sites are correlated with average coking rate (ACR) in Figure 8. The average coking rate (a.u./g·h) is identified as the consumption of oxygen per gram of used catalyst in an hour. From Figure 8, it is observed that the average coking rate of used Zn/HBeta was strongly related to the amount of total acid sites, especially the strong acid sites. To be specific, the higher the total amount of acid sites of the catalyst, the greater the average coking rate. These results indicate that the strong acid sites were mainly responsible for coke deposition, which was very consistent with the reported results [23]. In addition, the coke composition was also affected by the strength distribution of the acid sites. The FTIR results showed that a higher proportion of aromatic coke was deposited on the used Zn/HBeta-S, which was attributed to its relatively higher amount of strong acid sites. The side reactions, including but not limited to oligomerization, trimerization, cyclization and aromatization, would occur steadily on the strong acid sites. Generally, aromatic coke is difficult to remove, giving rise to catalyst deactivation. However, every coin has two sides. The precursors of aromatic coke were commonly used as active groups and/or the intermediates during the reaction. Madeira et al. found that the active groups included dehydrogenated species such as alkylated aromatics [5]. Thus, it can be reasonably explained that a higher propylene yield of as high as 19.0% was still retained for Zn/HBeta-S, with a larger amount of coke deposition after a TOS of 7 h.

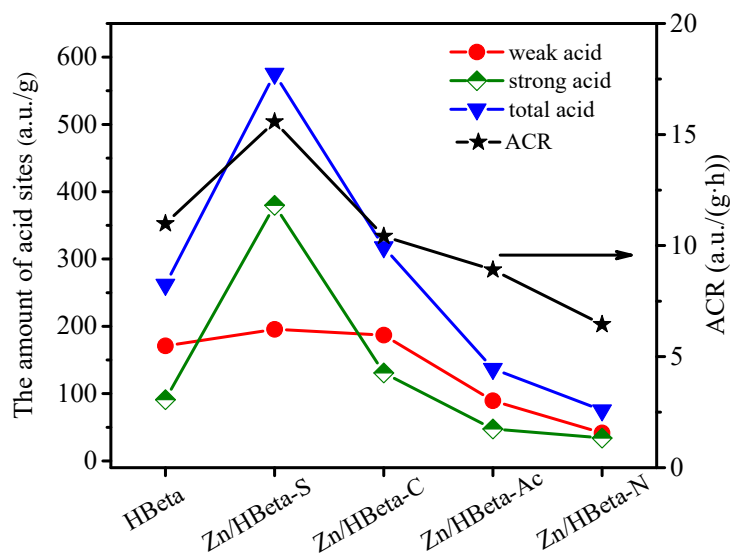


Figure 8. Correlations between acidic properties and average coking rate of the used Zn/HBeta catalysts.

4. Materials and Methods

4.1. Chemicals

All chemicals with analytical grade were directly employed as received without further purification. Zinc sulfate ($\text{ZnSO}_4 \cdot 7\text{H}_2\text{O}$), zinc chloride (ZnCl_2), zinc acetate ($\text{C}_4\text{H}_6\text{O}_4\text{Zn} \cdot 2\text{H}_2\text{O}$) and zinc nitrate ($\text{Zn}(\text{NO}_3)_2 \cdot 6\text{H}_2\text{O}$) were purchased from Shanghai Aladdin Biochemical Technology Co., Ltd., Shanghai, China. The HBeta zeolite (NKF-6-100H, Si/Al₂ molar ratio = 100) was purchased from Tianjin Nanhua Catalyst Co., Ltd., Tianjin, China.

4.2. Catalyst Preparation

A series of Zn/HBeta catalysts with 16 wt.% loading of zinc were prepared by the wetness impregnation method. Typically, a desired amount of zinc precursor was dissolved

in 50 mL of deionized water. The HBeta zeolite power was impregnated in an aqueous solution of different zinc precursors at 50 °C for 3 h. The impregnated power was dried at 110 °C for 12 h and then calcined at 450 °C for 4 h in air. The resulting Zn/HBeta catalysts were denoted as Zn/HBeta-S, Zn/HBeta-C, Zn/HBeta-Ac and Zn/HBeta-N, when $\text{ZnSO}_4 \cdot 7\text{H}_2\text{O}$, ZnCl_2 , $\text{C}_4\text{H}_6\text{O}_4\text{Zn} \cdot 2\text{H}_2\text{O}$ and $\text{Zn}(\text{NO}_3)_2 \cdot 6\text{H}_2\text{O}$ were used as the zinc precursor, respectively.

4.3. Catalyst Characterization

X-ray diffraction (XRD) patterns of the samples were obtained on a Rigaku Rotflex D/Max-C X-ray diffractometer (Tokyo, Japan) with a monochromatic $\text{Cu}/\text{K}\alpha$ radiation (40 kV, 30 mA). N_2 adsorption–desorption characterization was performed on a Micromeritics ASAP400 instrument (Norcross, GA, USA) at -196 °C. Prior to the adsorption, all the samples were pretreated under vacuum conditions at 300 °C for 6 h. The specific surface area was calculated according to the BET method. The micropore volume was obtained by *t*-plot analysis of the adsorption isotherm. The mesopore volume was obtained by the BJH method. The ammonia temperature-programmed desorption (NH_3 -TPD) and temperature-programmed oxidation (TPO) experiments were carried out on a self-built fixed-bed reactor system with gas chromatography (GC-3400, Beijing Beifen-Ruili Analytical Instrument Co., Ltd., Beijing, China). For NH_3 -TPD, the sample was pretreated in a N_2 flow at 200 °C for 2 h and then cooled down to 50 °C. The NH_3 was injected to the sample until adsorption saturation. The sample was purged in a N_2 flow to remove the physically adsorbed NH_3 from the sample surface. NH_3 -TPD was carried out from 50 to 600 °C with a heating rate of 10 °C min^{-1} in a N_2 flow. TPO was performed in an air flow from 50 to 800 °C with a heating rate of 10 °C/min. FTIR spectra of the samples were recorded by Nicolet FTIR 6700 spectrometer (Thermo Scientific, Waltham, MA, USA) with a resolution of 4 cm^{-1} .

4.4. Procedure for Evaluating the ETP Performance

The catalytic conversion of ethanol to propylene was carried out in a continuous-flow fixed-bed reactor. Prior to the evaluation, 0.5 g of catalyst (20–40 mesh) was pretreated in a N_2 flow at 400 °C for 30 min. The catalyst bed temperature was monitored by a K-type thermocouple in the catalyst bed. Ethanol was fed by a micro pump and vaporized. Ethanol and N_2 were mixed well and introduced into the reactor. The catalysts were evaluated under the reaction conditions of $T = 500$ °C, $P = 0.1$ MPa, $P_{\text{C}_2\text{H}_5\text{OH}} = 0.02$ MPa and $\text{WHSV} = 2.8$ h^{-1} . The outlet gas was analyzed by gas chromatography (GC-2060, Shanghai Ruimin Instrument Co., Ltd., Shanghai, China) with two analytical modules. The products were separated by a $\text{KB-Al}_2\text{O}_3/\text{Na}_2\text{SO}_4$ capillary column and detected by a flame ionization detector (FID) (Shanghai Ruimin Instrument Co., Ltd., Shanghai, China). Ethanol was identified by a GDX-103 packed column and detected by a thermal conductivity detector (TCD) (Agilent, Santa Clara, CA, USA). After the reaction, the used catalyst bed was swept with a N_2 flow (40 cm^3/min) for 30 min in order to stabilize and homogenize the coke deposited on used catalysts for further analysis. The ethanol conversion and the yield of products were calculated on a carbon basis. The specific calculation formula is as follows:

$$\text{Conversion of ethanol (\%)} = (\text{Ethanol}_{\text{in feed}} - \text{Ethanol}_{\text{in off-gas}}) / \text{Ethanol}_{\text{in feed}} \times 100\%$$

$$\text{Selectivity of product (\%)} = \text{Product} / \sum \text{Product} \times 100\%$$

$$\text{Yield of product (\%)} = \text{Conversion of ethanol} \times \text{Selectivity of product}$$

5. Conclusions

In summary, the amount and strength distribution of acid sites on the Zn/HBeta catalysts were simply tuned by introducing different types of zinc precursors, and further affected the propylene yield in the direct conversion of ethanol to propylene. Specifically, when the Zn species were introduced to the HBeta, the propylene yield was significantly enhanced, whereas the yields of ethylene and C_2 – C_4 alkane were remarkably suppressed.

In the case of the catalyst prepared using the ZnCl_2 precursor, Zn/HBeta-C showed a higher propylene yield of up to 43.3%, which was due to the moderate amount and strength distribution of acid sites. Both the total coke amount and the average coking rate of the used Zn/HBeta catalysts were closely associated with the amount of total acid sites, especially the strong acid sites. The higher the amount of total acid sites of the catalyst, the greater the total coke amount and average coking rate. For the catalyst prepared by using the $\text{ZnSO}_4 \cdot 7\text{H}_2\text{O}$ precursor, Zn/HBeta-S showed better stability, although its amount of coke deposition was higher after a TOS of 7 h, which was attributed to the higher amount of strong acid sites.

Author Contributions: Conceptualization, T.B. and B.C.; Methodology, T.B.; Software, X.L. and L.D.; Validation, T.B.; Formal analysis, X.L.; Investigation, T.B. and Y.-S.X.; Data curation, T.B.; Writing—original draft, T.B. and Y.-S.X.; Writing—review & editing, T.B. and Y.-S.X.; Visualization, J.W.; Supervision, B.C. All authors have read and agreed to the published version of the manuscript.

Funding: The research was funded by the Key Research and Development Program of Shaanxi province of China (2024SF-YBXM-613), Natural Science Basic Research Plan in Shaanxi Province of China (2022JQ-085) and Special Research Projects of Shaanxi Province of China (19JK0674).

Data Availability Statement: Data are contained within the article.

Conflicts of Interest: There are no conflicts to declare.

References

1. Matheus, C.R.V.; Aguiar, E.F.S. The role of MPV reaction in the synthesis of propene from ethanol through the acetone route. *Catal. Commun.* **2020**, *145*, 106096. [CrossRef]
2. Matheus, C.R.V.; Chagas, L.H.; Gonzalez, G.G.; Aguiar, E.F.S.; Appel, L.G. Synthesis of Propene from Ethanol: A Mechanistic Study. *ACS Catal.* **2018**, *8*, 7667–7678. [CrossRef]
3. Licht, R.B.; Bell, A.T. A DFT Investigation of the Mechanism of Propene Ammoxidation over α -Bismuth Molybdate. *ACS Catal.* **2016**, *7*, 161–176. [CrossRef]
4. Hussain, A.I.; Aitani, A.M.; Kubů, M.; Čejka, J.; Al-Khattaf, S. Catalytic cracking of Arabian Light VGO over novel zeolites as FCC catalyst additives for maximizing propylene yield. *Fuel* **2016**, *167*, 226–239. [CrossRef]
5. Phung, T.K.; Pham, T.L.M.; Vu, K.B.; Busca, G. (Bio)Propylene production processes: A critical review. *J. Environ. Chem. Eng.* **2021**, *9*, 105673. [CrossRef]
6. Song, S.; Sun, Y.; Yang, K.; Fo, Y.; Ji, X.; Su, H.; Li, Z.; Xu, C.; Huang, G.; Liu, J.; et al. Recent Progress in Metal-Molecular Sieve Catalysts for Propane Dehydrogenation. *ACS Catal.* **2023**, *13*, 6044–6067. [CrossRef]
7. Sun, J.; Wang, Y. Recent Advances in Catalytic Conversion of Ethanol to Chemicals. *ACS Catal.* **2014**, *4*, 1078–1090. [CrossRef]
8. Yin, J.; Guo, X.; Sun, Y.; Han, S.; Li, Q. Understanding the Nanoconfinement Effect on the Ethanol-to-Propene Mechanism Catalyzed by Acidic ZSM-5 and FAU Zeolites. *J. Phys. Chem. C* **2021**, *125*, 310–334. [CrossRef]
9. Huangfu, J.; Mao, D.; Zhai, X.; Guo, Q. Remarkably enhanced stability of HZSM-5 zeolite co-modified with alkaline and phosphorous for the selective conversion of bio-ethanol to propylene. *Appl. Catal. A Gen.* **2016**, *520*, 99–104. [CrossRef]
10. Duan, C.; Zhang, X.; Zhou, R.; Hua, Y.; Zhang, L.; Chen, J. Comparative studies of ethanol to propylene over HZSM-5/SAPO-34 catalysts prepared by hydrothermal synthesis and physical mixture. *Fuel Process. Technol.* **2013**, *108*, 31–40. [CrossRef]
11. Xia, W.; Chen, K.; Takahashi, A.; Li, X.; Mu, X.; Han, C.; Liu, L.; Nakamura, I.; Fujitani, T. Effects of particle size on catalytic conversion of ethanol to propylene over H-ZSM-5 catalysts—Smaller is better. *Catal. Commun.* **2016**, *73*, 27–33. [CrossRef]
12. Xia, W.; Takahashi, A.; Nakamura, I.; Shimada, H.; Fujitani, T. Study of active sites on the MFI zeolite catalysts for the transformation of ethanol into propylene. *J. Mol. Catal. A Chem.* **2010**, *328*, 114–118. [CrossRef]
13. Li, X.; Kant, A.; He, Y.; Thakkar, H.V.; Atanga, M.A.; Rezaei, F.; Ludlow, D.K.; Rownaghi, A.A. Light olefins from renewable resources: Selective catalytic dehydration of bioethanol to propylene over zeolite and transition metal oxide catalysts. *Catal. Today* **2016**, *276*, 62–77. [CrossRef]
14. Xia, W.; Wang, J.; Wang, L.; Qian, C.; Ma, C.; Huang, Y.; Fan, Y.; Hou, M.; Chen, K. Ethylene and propylene production from ethanol over Sr/ZSM-5 catalysts: A combined experimental and computational study. *Appl. Catal. B Environ.* **2021**, *294*, 120242. [CrossRef]
15. Zhang, N.; Mao, D.; Zhai, X. Selective conversion of bio-ethanol to propene over nano-HZSM-5 zeolite: Remarkably enhanced catalytic performance by fluorine modification. *Fuel Process. Technol.* **2017**, *167*, 50–60. [CrossRef]
16. Huang, R.; Fung, V.; Wu, Z.; Jiang, D.-E. Understanding the conversion of ethanol to propene on In_2O_3 from first principles. *Catal. Today* **2020**, *350*, 19–24. [CrossRef]
17. Wang, F.; Xia, W.; Mu, X.; Chen, K.; Si, H.; Li, Z. A combined experimental and theoretical study on ethanol conversion to propylene over Y/ZrO₂ catalyst. *Appl. Surf. Sci.* **2018**, *439*, 405–412. [CrossRef]

18. Xia, W.; Wang, F.; Mu, X.; Chen, K. Remarkably enhanced selectivity for conversion of ethanol to propylene over ZrO₂ catalysts. *Fuel Process. Technol.* **2017**, *166*, 140–145. [[CrossRef](#)]
19. Hayashi, F.; Iwamoto, M. Yttrium-Modified Ceria As a Highly Durable Catalyst for the Selective Conversion of Ethanol to Propene and Ethene. *ACS Catal.* **2012**, *3*, 14–17. [[CrossRef](#)]
20. Hayashi, F.; Tanaka, M.; Lin, D.; Iwamoto, M. Surface structure of yttrium-modified ceria catalysts and reaction pathways from ethanol to propene. *J. Catal.* **2014**, *316*, 112–120. [[CrossRef](#)]
21. Iwamoto, M.; Tanaka, M.; Hirakawa, S.; Mizuno, S.; Kurosawa, M. Pulse and IR Study on the Reaction Pathways for the Conversion of Ethanol to Propene over Scandium-Loaded Indium Oxide Catalysts. *ACS Catal.* **2014**, *4*, 3463–3469. [[CrossRef](#)]
22. Xue, F.; Miao, C.; Yue, Y.; Hua, W.; Gao, Z. Direct conversion of bio-ethanol to propylene in high yield over the composite of In₂O₃ and zeolite beta. *Green Chem* **2017**, *19*, 5582–5590. [[CrossRef](#)]
23. Xu, L.; Zhao, R.; Zhang, W. One-step high-yield production of renewable propene from bioethanol over composite ZnCeOx oxide and HBeta zeolite with balanced Brønsted/Lewis acidity. *Appl. Catal. B Environ.* **2020**, *279*, 119389. [[CrossRef](#)]
24. Jin, H.; Yue, Y.; Miao, C.; Tian, C.; Hua, W.; Gao, Z. Direct and Highly Selective Conversion of Bioethanol to Propylene Over Y-CeO₂ and Zeolite Beta Composite. *Catal Lett* **2022**, *153*, 230–238. [[CrossRef](#)]
25. Xue, F.; Miao, C.; Yue, Y.; Hua, W.; Gao, Z. Sc₂O₃-promoted composite of In₂O₃ and Beta zeolite for direct conversion of bio-ethanol to propylene. *Fuel Process. Technol.* **2019**, *186*, 110–115. [[CrossRef](#)]
26. Islam, M.J.; Granollers Mesa, M.; Osatiashiani, A.; Taylor, M.J.; Manayil, J.C.; Parlett, C.M.A.; Isaacs, M.A.; Kyriakou, G. The effect of metal precursor on copper phase dispersion and nanoparticle formation for the catalytic transformations of furfural. *Appl. Catal. B Environ.* **2020**, *273*, 119062. [[CrossRef](#)]
27. Shao, B.; Ren, K.; Zhang, C.; Lin, M.; Zhou, S.; Li, Y.; Zong, B. Effect of Metal Precursors on the Performance of Pt/Y Catalysts for Isobutane-Butene Alkylation Reaction-Regeneration. *Ind. Eng. Chem. Res.* **2023**, *62*, 19619–19628. [[CrossRef](#)]
28. Rehman, A.U.; Khan, M.; Maosheng, Z. Hydration behavior of MgSO₄-ZnSO₄ composites for long-term thermochemical heat storage application. *J. Energy Storage* **2019**, *26*, 101026. [[CrossRef](#)]
29. Kurban, G.V.T.; Rego, A.S.C.; Mello, N.M.; Brocchi, E.A.; Navarro, R.C.S.; Souza, R.F.M. Thermodynamics and Kinetic Modeling of the ZnSO₄·H₂O Thermal Decomposition in the Presence of a Pd/Al₂O₃ Catalyst. *Energies* **2022**, *15*, 548. [[CrossRef](#)]
30. Liao, W.; Tang, C.; Zheng, H.; Ding, J.; Zhang, K.; Wang, H.; Lu, J.; Huang, W.; Zhang, Z. Tuning activity and selectivity of CO₂ hydrogenation via metal-oxide interfaces over ZnO-supported metal catalysts. *J. Catal.* **2022**, *407*, 126–140. [[CrossRef](#)]
31. Zhang, B.; Zhu, X.; Gao, J.; Zhu, Y.; Ma, W. Zn modification of Beta zeolite: Effect on acid sites and propylene oxide rearrangement. *Chem. Phys.* **2020**, *539*, 110983. [[CrossRef](#)]
32. Bai, T.; Zhang, X.; Wang, F.; Qu, W.; Liu, X.; Duan, C. Coking behaviors and kinetics on HZSM-5/SAPO-34 catalysts for conversion of ethanol to propylene. *J. Energy Chem.* **2016**, *25*, 545–552. [[CrossRef](#)]
33. Sousa, Z.S.B.; Cesar, D.V.; Henriques, C.A.; Teixeira da Silva, V. Bioethanol conversion into hydrocarbons on HZSM-5 and HMCM-22 zeolites: Use of in situ DRIFTS to elucidate the role of the acidity and of the pore structure over the coke formation and product distribution. *Catal. Today* **2014**, *234*, 182–191. [[CrossRef](#)]
34. Pinard, L.; Tayeb, K.B.; Hamieh, S.; Vezin, H.; Canaff, C.; Maury, S.; Delpoux, O.; Pouilloux, Y. On the involvement of radical “coke” in ethanol conversion to hydrocarbons over HZSM-5 zeolite. *Catal. Today* **2013**, *218–219*, 57–64. [[CrossRef](#)]
35. Ferreira Madeira, F.; Ben Tayeb, K.; Pinard, L.; Vezin, H.; Maury, S.; Cadran, N. Ethanol transformation into hydrocarbons on ZSM-5 zeolites: Influence of Si/Al ratio on catalytic performances and deactivation rate. Study of the radical species role. *Appl. Catal. A Gen.* **2012**, *443–444*, 171–180. [[CrossRef](#)]

Disclaimer/Publisher’s Note: The statements, opinions and data contained in all publications are solely those of the individual author(s) and contributor(s) and not of MDPI and/or the editor(s). MDPI and/or the editor(s) disclaim responsibility for any injury to people or property resulting from any ideas, methods, instructions or products referred to in the content.